Experimental and Numerical Investigation of Flash-butt-welded Joints in Pearlitic-steel Rails: Fatigue and Residual Stress

Rodrigo Rangel Porcaro[a]* (ID), **Leonardo Barbosa Godefroid**[a] (ID), **Francisco Célio de Araújo**[a],

Geraldo Lúcio de Faria[a], **Luiz Cláudio Cândido**[a]

[a]Universidade Federal de Ouro Preto, Ouro Preto, MG, Brasil.

This study is focused on the performance evaluation of flash-butt-welded rail joints concerning their mechanical strength and fatigue life. Residual stresses created in the heat-affected zone were measured and the effects of the welding process and notch sensitivity on the fatigue behavior in the weld region were experimentally assessed. Aiming at clarifying the physical phenomenon behind the flash-butt welding, nonlinear transient thermomechanical finite-element analyses were performed to reconstitute the welding process and to simulate the subsequent formation of residual stresses. A new hypothesis for explaining higher temperatures in the rail web than in the rail foot and head was suggested and numerically verified. Experimental fatigue results showed high notch sensitivity and highlighted the effects of microstructure variations on the fatigue life. In general, a good agreement was achieved between numerical and experimental measurements of residual stresses, which was essential for understanding the fatigue phenomenon and the formation of residual stresses in flash-butt-welded rail joints. A relevant outcome is the simulation of the hot burrs from the welding process as prescribed heat inputs on a convenient part of the rail surface. This simulation strategy has shown adequate to explain the non-uniform temperature changes and the corresponding originated residual stresses.

Keywords: *Flash-Butt Welding (FBW), Fatigue of Welded Joints, Residual Stresses, Notch Sensitivity, Nonlinear Transient Thermal, Thermomechanical Analysis.*

1. Introduction

Nowadays, most railway tracks worldwide are built using continuously welded rails (CWRs) formed by flash-butt welding individual rail segments. By reasons of increasing axle loads, higher speeds, and heavier traffic of trains—as a consequence of the increasing demand for transportation of goods and people—it is fundamental to assure the structural integrity of the railways. In this context, the welds play an important role as they are regions of mechanical weakness within the CWR that are usually associated with failure sources in the lifetime of railways[1].

As flash-butt welding (FBW) is a solid-state joining method, a burr will be formed during the process. A common practice currently adopted to remove it from the welded surface is to cut off the hot burr immediately after the welding, and then to cold-grind only the head and foot surfaces of the rail[1]. For reference, the British Standard EN 14587-1[2] establishes as acceptable, after the FBW process has finished, burrs up to 2mm on the rail web surface.

Farhangi and Mousavizadeh[3] have identified a macroscopic fatigue cracking pattern in FBW joints having the following characteristics: crack initiating in the web surface, propagating initially parallel to the rolling surface and then towards the head and foot of the rail. Based on metallographic analysis, the authors concluded that this failure mode was caused by fatigue crack nucleation in the web surface of the rails, triggered by some stress concentrators, such as burrs from the welding process or oxide inclusions inserted by the deburring tool. In addition, residual tensile stresses in the web, resulting from the FBW process, were appointed as early fatigue-failure facilitators. This phenomenon was also studied by Desimone and Beretta[4], who defined it as Horizontal Split Web (HSW) fatigue-failure mode.

Haibatollahi and Tehrani[5] reported high values of tensile residual stresses in the web of rail joints after the FBW process. Skittebol et al.[6] evaluated how the residual stress states resulting from the flash-butt welding process influenced the fatigue crack growth in the HSW failure mode. Mansouri and Monshi[7] attributed the development of residual stresses during the flash-butt welding to a higher electric current density in the rail web, which was related to a greater area/volume relationship in that region than in the rail head and foot. In a recent work[8], the authors monitored the evolution of temperatures in all rail regions during the FBW process. The reported results corroborated the hypothesis raised previously[7] because the peak temperature in the rail web was higher than 1400°C, while it did not exceed 1355°C in its head and foot. Tawfik et al.[9] suggested rapid post-welding heat treatments to reduce the level of residual stresses caused by flash-butt welding in rails and presented numerical results associated with their strategies.

*e-mail: rodrigo.porcaro@ufop.edu.br

Godefroid et al.[10] have presented detailed studies of recurrent failures on flash-butt-welded rails. These authors attributed the failures to fatigue with crack nucleation caused by stress concentrators formed due to inadequate deburring in the web and foot of the joints. In addition, structural changes in the material as a result of thermal welding cycles, mainly decarburization and partial spheroidization of the cementite, were also identified as responsible for facilitating the early nucleation of fatigue cracks.

Other issues pointed out by Mansouri and Monshi[7] and Porcaro et al.[11] were the structural changes resulting from the flash-butt welding of pearlitic rails. These authors identified three different regions composing the heat-affected zone (HAZ) of joints with the following characteristics: grain growth, grain refining as a result of recrystallization, and partial phase transformation. The structural changes, also reported by Micenko et al.[12], included partial decarburization and a large variation of hardness in the partial transformation region because of cementite spheroidization. Besides, the variations in hardness in the rail head after the flash-butt welding can cause localized wear or plastic strain during the railway lifetime[13], which, in turn, increases the vibrations associated with fatigue[14].

As discussed by Zhao et al.[15], although fatigue is the main responsible for failures in continuously welded rails, there are only few studies showing fatigue data at flash-butt-welded rail joints. One notable exception is the recent work published by Sarikavak et al.[16], in which they carry out a 4-point bending test and obtain fatigue data at the head, web, and foot subsections of a flash-butt-welded rail.

In this context of lack of knowledge about the fatigue behavior of FBW joints, this paper presents a detailed mechanical characterization of flash-butt-welded joints of pearlitic-steel rails, including their experimental assessment based on residual stresses and fatigue. Furthermore, nonlinear transient thermal and thermomechanical finite-element (FE) analyses were employed to reconstitute the whole FBW process and to describe the subsequent formation of residual stresses.

In this respect, the hot burrs from the welding process have been simulated in a more appropriate way—as prescribed heat inputs—to clarify the physical FBW process. In addition, essential information was provided about the material's strength concerning fatigue initiation at the base metal and in the flash-butt welded joints (including stress concentration effects). Notice that the material constitutive laws incorporated into the FE models, which also describe the material fatigue behavior in the weld, will allow more accurate investigations of flash-butt-welded CWRs under combined action of moving trains and thermal loads.

2. Materials and Methods

2.1. Materials

In this study, a pearlitic steel for railroad application was considered, classified as an intermediate steel according to the AREMA (2013) Standard[17], whose tensile and hardness mechanical properties specifications are given in Table 1. A TR57 profile was considered in the tests, which weighs 57kg/m. The rails correspond to a single batch of material and were welded in a Brazilian stationary flash-butt welding facility according to the parameters presented in Table 2, in segments of 25 m length. No accelerated cooling was applied after welding. In a previous paper[11], a detailed metallographic characterization of the base metal and welded joints was presented.

2.2. Surface residual stresses

The superficial residual stress measurements were performed in the welded joints by the hole-drilling strain gauge method according to the ASTM E837[18] Standard. Three welded joints were analyzed according to the positions indicated in Figure 1a. Figure 1b shows an example of the assembly used in the drilling process. Three measurements for each point in Figure 1a were made in the flash-butt-welded joints.

The drilling process was performed in 0.05-mm increments, until the total depth of 1 mm, by employing a dental cone drill having 1.59-mm diameter. The measurements in the tests were carried out by using KFG-1.5-120-D28-11 strain gages from Kyowa (manufacturer). The H-Drill® software was finally applied to process all the obtained data as well as to check the validity of the measurements and to determine the residual stresses according to the ASTM E837[18] Standard. In the calculations, a Young's modulus of 208GPa and a Poisson's ratio equal to 0.3 were considered for the pearlitic steel[5,9]. The yield strength was obtained from tensile tests in welded joints.

Table 1. Mechanical properties specifications for intermediate*steel rail.

Mechanical Properties	Minimum required
Yield strength (MPa)	551
Tensile strength (MPa)	1013
Elongation at fracture (%)	8
Superficial Hardness (HB)	325

* – The "intermediate" is a classification between the standard and the high strength (AREMA[17]).

Table 2. Controlled parameters for the flash butt welding of the TR57 intermediate steel rail, segments with 25 m length.

| Controlled parameter during welding	Values	
Intensity and duration of the initial flash	77.4kA	20s
Number of preheat current pulses and pulse duration	10un.	3.8s
Intensity of the preheat pulses	45-70kA	-
Force intensity during the preheating pulses	106kN	-
Intensity and duration of the final flash	38.3kA	14.4s
Intensity of final force	477kN	-
Total displacement	37-45mm	-
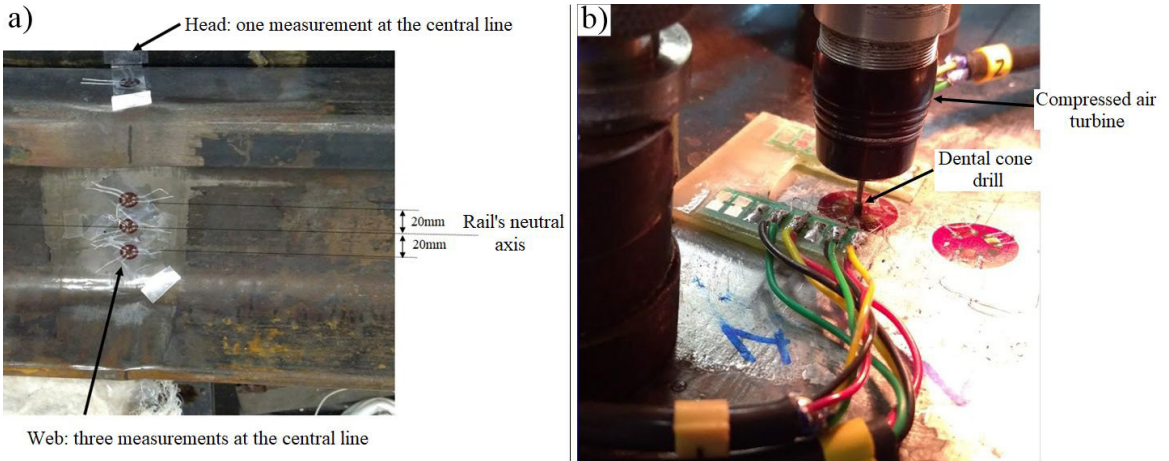
Figure 1. (a) Locations for measurement of residual stresses in flash-butt-welded rail joints. (b) Example of the experimental setup used in the drilling process and a strain gauge rosette glued on the surface.

2.3. Tensile and fatigue mechanical tests

For the uniaxial tensile tests, three specimens from the base metal and three specimens from the welded joints were evaluated according to the ASTM E8M[19] Standard. These specimens were longitudinally sampled from the rail head, at positions 10 mm below the rolling surface, and machined with the dimensions presented in Figure 2a. Particularly in the case of the specimens taken from the flash-butt-welded joints, they were etched with Nital 4% to ensure that the full extent of the HAZ was confined inside the gage length (Figure 2b). The used gage length was larger than the total width of the HAZ (about 30 mm). Another group of tensile tests was carried out to quantify the notch effect on the welded joints. In this case, the notch shown in Figure 2c, with 0.8-mm radius and 0.4-mm depth, was machined at the end of the HAZ (partial transformation region[11]). The notch geometry aimed at introducing the effects of the burr on the surface of the flash-butt-welded joints after the welding process[1].

For the fatigue tests, the same geometry presented in Figure 2 was used, and the tests were performed in three comparative groups: (i) base metal, (ii) welded joints without notch, and (iii) welded joints with a notch in the partial transformation (or spheroidization[11]) region of the HAZ (see Figure 2c). Based on previous works[1,10,11] and in the tolerance for the burr removal[2], the notch is used to simulate the stress concentration at the end of the HAZ, which is, in turn, associated with the HSW fatigue failure mode. The stress-controlled tests were carried out in a servo-hydraulic Instron machine with 250-kN capacity and following ASTM E466 Standard[20].

The samples for the fatigue tests were also extracted from the rail heads at 10 mm below the rolling surface. In the tests, a stress ratio of 0.1 and a sinusoidal loading with a frequency of 30 Hz were adopted (constant amplitude loading). The load level started at 90% of the tensile strength, in each case, and was decreased by amounts of 10% until a fixed fatigue limit has been achieved (10^7 cycles). Three samples were tested for each load level, at room temperature.
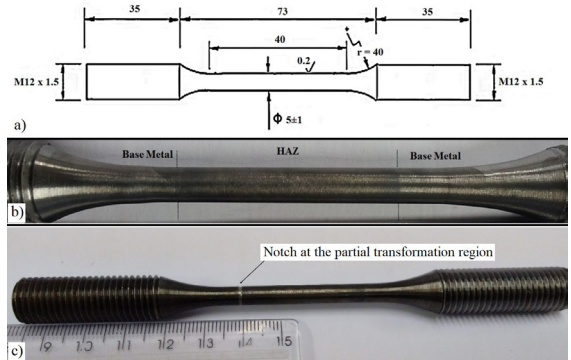

Figure 2. Specimen for the tensile and fatigue tests. (a) Specimen dimensions (mm); (b) specimen from the welded joint etched with Nital 4% highlighting the HAZ; (c) specimen from the welded joint with a notch at the end of the HAZ (partial transformation region).

2.4. Numerical analysis

The development of residual stresses during the FBW process was simulated with the finite-element method (FEM). In this study, the ANSYS 17.0 software[21] was used. The first part of the simulation was to generate the 3D-geometry of the models by considering the geometrical details stated according to the AREMA specifications[17].

Figure 3 shows the 260-mm-long finite-element model adopted in the simulations, which is formed by a mesh having 34,600 10-node tetrahedron elements, making up a total of 52,000 nodes. The mesh in the region of the weld is refined to allow a convenient reconstitution of physical variables having higher gradients. A mesh-refinement study was performed and the mesh quality parameters were checked. The 260-mm length of the model is enough to capture the thermal gradient during the simulated welding process (the minimum temperature did not change at model's end).

The simulation was divided into two steps: (i) a nonlinear transient thermal analysis for obtaining the time-dependent temperature distribution, in a TR57 rail, corresponding to

the FBW process; (ii) the quasi-static thermomechanical structural analysis to evaluate the stress states resulting from the residual stresses (originated in the FBW process). In the computational analyses, displacement restrictions were imposed at the model ends to simulate the neighboring rail elements.

As a result of the welding process, the model experiences relatively small shape distortions[5,9]. Thus, an uncoupled thermal and mechanical analysis may be satisfactorily applied. In other words, the nonlinear heat conduction problem to evaluate the time-dependent temperature distribution along the rail is firstly solved, and then, the resulting residual stresses are determined[22]. In this way, the total CPU time for the analysis is reduced if compared to the coupled thermomechanical analysis, as made by previous researchers[5,6,8,23-25].

To assure the correct evaluation of the strain and stress distributions in the welded rails, a material model has been incorporated into the ANSYS software. In that model, the same nonlinear temperature-dependent thermal conductivity and heat capacity adopted by Cai et al.[23] were considered. Ma et al.[25] reported a significant effect of phase transformations on the residual stress profile of flash-butt-welded rails, however, they considered the formation of martensite as the main influential factor. Since the reported cooling rate of that process was around 1°C/s[8] and only pearlite was obtained during the characterization of the joints[11], phase transformations were not considered in the material model (similar to Skyttebol et al.[6]). Here, an instantaneous thermal expansion coefficient equal to 3×10^{-5}/°C was adopted, which was obtained from the derivative of the relative strain experimentally measured in dilatometric tests[11].

The bilinear isotropic hardening model from ANSYS[21] was used to describe the material parameters as a function of the temperature. The same temperature-dependent material constitutive laws employed by Haibatollahi and Tehrani[5] were adopted because the steel considered in that study was similar to the intermediate one considered here. If the objective of the analysis were to study surface fatigue due to the wheel passage, a different material model should be used to simulate the cyclic plasticity. Nevertheless, in the present analysis, only the part well below the surface of the rail head is investigated, and so, the bilinear isotropic hardening is sufficient. A similar approach was employed by Skyttebol et al.[6].

2.4.1. Thermal analysis

As mentioned above, the nonlinear time-dependent thermal analysis is carried out to determine the thermal loading (thermal cycles) originated from the welding process to be considered, later on, in the calculation of the residual stresses. Here, an equivalent volume heat source in the weld region was considered. The analysis was carried out by using the transient thermal module from the ANSYS. The 'SOLID 87' finite element (parabolic 10-node tetrahedron element) was employed.

In previous works, Masouri and Monshi[7], Weingrill et al.[8] and Porcaro et al.[1] showed that the highest temperatures during the FBW process occurred in the web of the rail cross section, which is a fundamental aspect to explain the high levels of vertical normal residual stresses at the

web of flash-butt-welded joints. Furthermore, as shown by Porcaro et al.[26], the temperature distribution model must take into account the fact that, in the weld region, the temperatures on the rail surface should be higher than inside of the rail (also stated by Mansouri and Monshi[7]).

Based on these assumptions and considering the welding parameters shown in Table 2, a volume heat source was applied to the model for 80s using a 30-mm-wide volume centered around the rail interfaces (see Figure 4). Different values of heat densities were tested so as to state the heat input values corresponding to the real welding process. The calibration of the transient heat source (heat density in W/mm^3) was based on the following criteria: (i) the width of the heated region above 727°C should be similar to that measured in the macrographic analyses of the HAZ in welded joints; (ii) the peak temperatures at the web, head and foot of the rail should be similar to those reported previously[8]; (iii) the cooling rate after finishing the flash-butt welding should be about 1°C/s (from 800°C to 500°C) as observed from the dilatometric analyses of the steel[11]. Such assumptions resulted in a volume heat source of $0.125 W/mm^3$ in the rail head and foot, and of $0.140 W/mm^3$ in the rail web, acting for 80s. During this same time, a surface heat input equal to $0.1 W/mm^2$ was applied to the boundary of the weld region (see Figure 4).
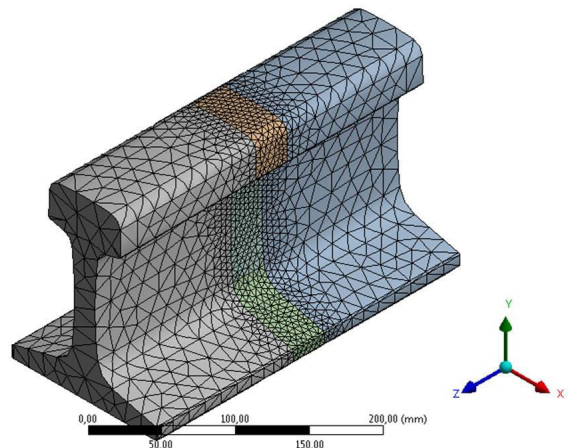

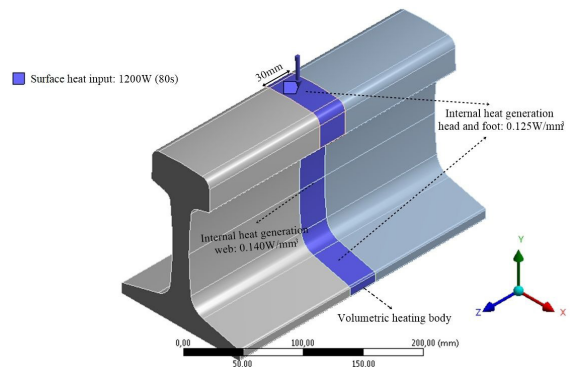**Figure 3.** 3D finite-element model for the welded rail joint.

Figure 4. Boundary conditions associated with the FBW process of a TR57 steel rail.

These boundary conditions were based on macrographic analyses of welded joints and will be discussed further in this paper. In addition, normal heat fluxes were set to zero at the rail ends and an initial 25°C temperature was assumed throughout the model.

Convection and radiation boundary conditions were considered all over the rest of the model surface, except at the end cross sections (XY planes) and at the surface confining the weld region (blue surface in Figure 4). The same convection coefficient adopted by Ma et al.[25] has been considered here. The used radiation model was that from ANSYS17.0, based on a 25°C room temperature[21]. To perform the time-domain thermal analysis, time increments of 0.1s were adopted.

2.4.2. Structural analysis

In the structural analysis, the previously determined time-dependent temperature distribution throughout the model was applied as thermal loading to the structural analysis model to predict the residual stresses after the welding. The calculations have been performed by utilizing the ANSYS static structural module[21]. The boundary conditions imposed to the mechanical model are shown in Figure 5a. In the XY plane (A) in Figure 5, all displacements were restrained because, during the FBW process, the fixed electrode restricts all movements of the rail. On the other hand, at the end plane of the model opposite to the A plane (see in Figure 5), a distributed elastic support with stiffness of 200N/mm^3—adjusted after some trials—was adopted to simulate the rail connected to the mobile electrode during the flash-butt welding. Besides, the common region between the rail parts has been modeled as a "shared topology"[21], which means that the analysis model comprises perfectly coupled substructures. As usual, the force applied at the end of the welding process has been neglected in the simulation[5,8,23,25].

Consistently with the thermal analysis, the residual stresses are evaluated by conducting a 3D materially nonlinear quasi-static thermomechanical analysis by employing the 'SOLID 187' finite element (parabolic 10-node tetrahedron finite element) from the software[21].

3. Results and Discussion

3.1. Experimental investigation

3.1.1. Surface residual stresses

Figure 6a presents the normal components of the surface residual stresses measured at the four points highlighted in the Figure 6b. It is worth mentioning that the shear components of the residual stresses on the surface of welded joints are negligible. Thus, for practical purposes, the residual stresses are characterized by their normal stress components[7].

The experimental residual stresses obtained in the welded joints of pearlitic-steel rails followed the same pattern of previous works[6,23,24], with tensile normal stresses observed in the vertical and longitudinal directions of the web, and compressive normal stresses at the head of the joints. The residual stresses can be explained by the occurrence of intense plastic deformations during the welding that remains left after the process has been finished.

In the heating cycle, the expansion of the web region, which undergoes temperatures higher than the ones in the head and foot of the rail, is restrained. After the cooling stage, the material experiences shrinkage and some positive elastic strains are left in the web region, originating tensile stresses, which are counterbalanced by compressive stresses in the head and foot of the rail joint[27].

Different values of residual stresses in flash-butt-welded rail joints have been reported in the literature[5,7,9,23-25]. However, as the residual stress level depends on a series of welding parameters, post-welding cooling conditions, the chemical composition of the rail steel, and the employed measurement techniques, it is reasonable to assume that different residual stress values may be obtained for different welded joints[28].

It is well known that residual tensile stresses associated with stress concentrations due to the welding burrs in the web surface of the welded joint are responsible for the occurrence of premature failures associated with horizontal split web fatigue in flash-butt-welded rail joints[6,10,29]. One of the most important aspects related to residual stresses originating in the web of flash-butt-welded rail joints is the fact that this stress state practically does not change during the life cycle of the component, even though it undergoes high external loading due to the traffic of trains[6].
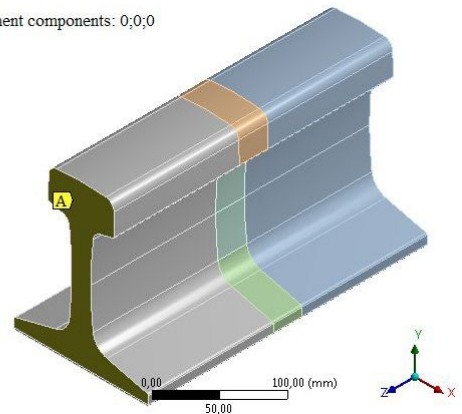

Figure 5. Thermomechanical analysis model during FBW.
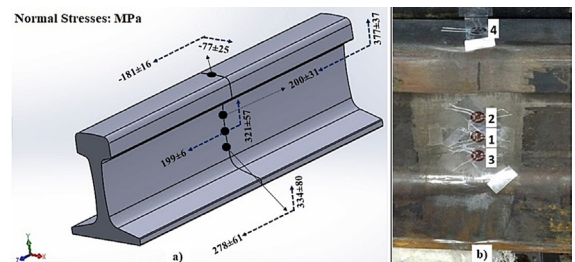

Figure 6. (a) Average values of normal residual stresses (MPa) obtained from the hole-drilling strain-gauge method in FBW steel rails (see the reference axis). (b) Measurement points of residual stresses at the web (1,2,3) and head section (4) of the rail.
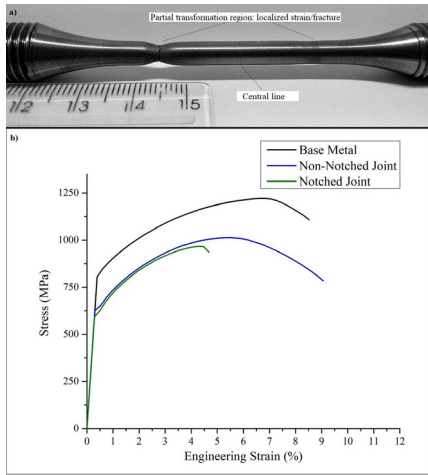
Figure 7. (a) Fractured tensile specimen of the FBW joint in an intermediate pearlitic steel rail(b) Stress-strain curves obtained in tensile tests for the base metal and for non-notched and notched FBW joints.

3.1.2. Mechanical tests

The results of tensile tests of the base metal, non-notched welded joints, and notched welded joints are presented in Table 3. The base metal fulfills the specifications stated by the AREMA[17]. However, regarding the welds, an average decrease of 17% in the yield strength and 13% in the tensile strength was observed, accompanied by a small increase in the percent elongation. In addition, as illustrated in Figure 7(a), all specimens from the welded joints fractured in the partial transformation region, which is a phenomenon that takes place because of the partial cementite spheroidization[1,11], see Figure 8. Similar results were reported by Sarikavak et al.[16] and, considering premium steel rails, by Bauri et al.[30].

Examples of engineering curves obtained in the tensile tests are shown in Figure 7b. One can see that the notch in the HAZ of the specimens had a significant effect in reducing the yield strength, tensile strength, and the elongation compared to the non-notched welded specimens (see also Table 3).
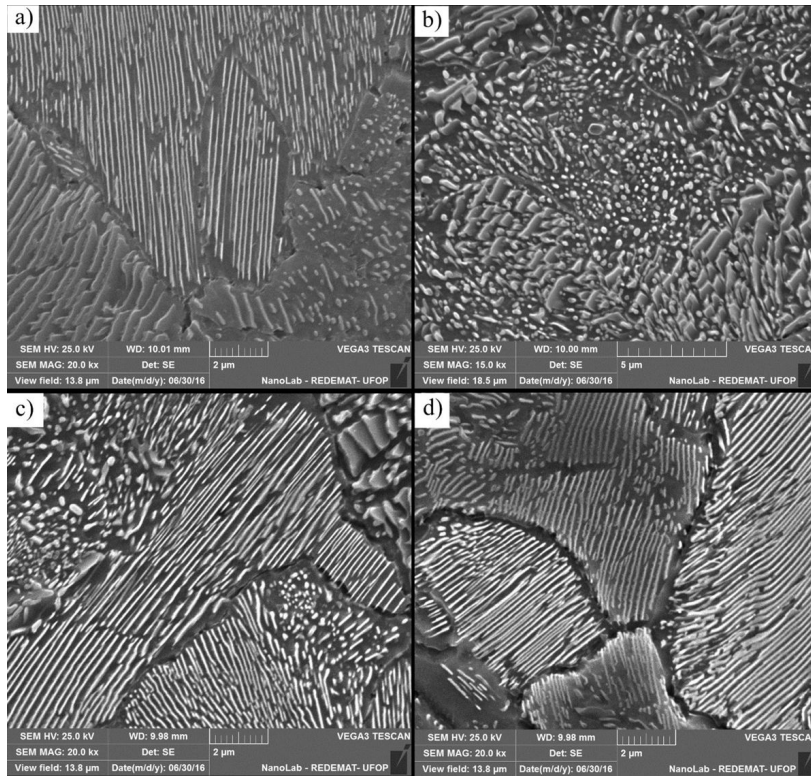

Figure 8. SEM-Microstructures of FBW intermediate pearlitic steel rail (a) base metal, 18-mm from the central line; (b) partial spheroidized region, 12-mm from the central line; (c) recrystallization: fine grain region, 8-mm from the central line; grain growth region, 2-mm from the central line. Adapted from Porcaro *et al.*[1].

Table 3. Tensile test results from the base metal, non-notched and notched welded joints.

Condition	Yield Strength (MPa)	Tensile Strength (MPa)	Elongation at Fracture (%)
Base Metal	768±32	1185±31	9±3
Non-notched Welded Joint	639±13	1035±19	10±1
Notched Welded Joint	573±17	950±14	4.0±0.5

The results of fatigue evaluation are comparatively shown in Figure 9 as S-N or Wöhler curves. The FBW process significantly worsened the steel fatigue performance when compared to the base metal, both in the low-cycle fatigue (LCF) and high-cycle fatigue (HCF) regimes. In both cases, three specimens showed the maximum fatigue life (more than 10^7 cycles) when the maximum applied stress corresponded to 50% of the tensile strength. However, from the point of view of the stress amplitudes, the corresponding values for the base metal and the welded joint were of 261MPa and 218MPa, respectively. The welding process reduced then the fatigue limit of the steel by approximately 16%. Thus, this effect must be obviously considered in the design and maintenance planning of CWRs.

The influence of the notch on the fatigue life of welded joints must also be emphasized. As seen in Figure 9, the notch effect is significantly higher in the HCF regime, whereas it is less significant in the LCF regime. These results are very relevant, because the current practice in FBW facilities, all over the world, is not to recommend removing welding burrs left on the web surface of welded rail joints. Thus, as proposed in previous works[10,29], stringent finishing processes should be accomplished all over the FBW regions. During the fatigue tests of notched samples, due to the high dispersion observed in the results with the minimum stress amplitude (Figure 9), 4 samples were tested. For all the other conditions shown in Figure 9, three samples were tested.

From all the samples taken from welded joints that failed in the fatigue tests (a total of 15 specimens), only two exhibited fracture at the central line. The majority of the failures occurred in the partial transformation region. Therefore, the decrease of material resistance to fatigue crack nucleation can be attributed to the pearlite microstructural modifications in the partial transformation region of the HAZ[11]. This behavior is related to the loss of mechanical strength of the partial spheroidized region. In this region extrusion and intrusion areas are formed during the cyclic loadings, giving rise then to stress concentrations and the consequent nucleation of fatigue microcracks[31].
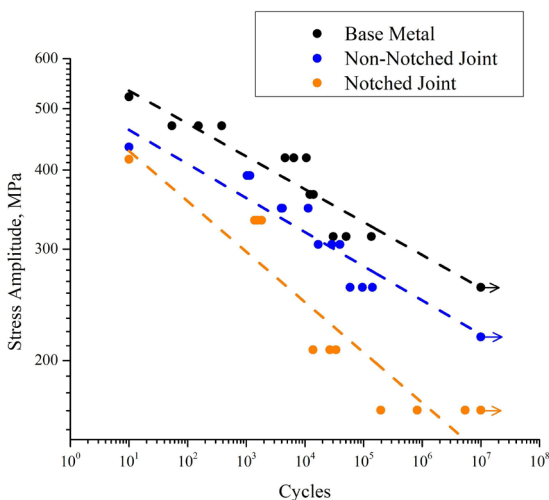
Sarikavak et al.[16] evaluated the fatigue life of FBW rails using 4-point bending fatigue tests. They observed that all samples extracted from the rail head section fractured at the end of the HAZ—the same critical location found here, although in the present study only axial tensile fatigue tests were carried out. As stated by Salehi et al.[32], the evaluation of fatigue parameters for welded rails using conventional fatigue tests requires a large number of cylindrical specimens. Here, more than 40 specimens were used, which correspond to 16 flash-butt-welded joints.

The experimental fatigue data presented here is very significant, as an example, one can see the work published by Salehi et al.[32] which numerically evaluated the fatigue performance of welded rail joints. Despite the complex numerical models adopted in that paper, which took into account multiaxial fatigue analyses, the fatigue properties used for the materials were very simple, based on hardness or tensile tests, since there were no experimental fatigue data available[32].

In this study, the two samples that fractured at the central line were submitted to a high-cycle fatigue regime. A similar mechanism considered for explaining the fracture in the partial transformation region was adopted here as well, with the ferrite at the central line[11] being the plastic deformation facilitator. Another possible failure cause could be the presence of welding defects. However, they were not found during the characterization of the welded joints. Noteworthy, the loss of resistance to fatigue due to crack nucleation was more significant in the partial transformation region.

Fractographic analyses of samples taken from the fatigue tests were conducted by using a Scanning Electron Microscope (SEM). The results are exemplified in Figure 10 for the base metal, in which high-cycle fatigue is considered with the maximum tensile stress corresponding to 60% of the tensile strength and a life of 50,376 cycles. Figure 10a clearly shows the regions of fatigue crack nucleation and stable propagation. The nucleation region is highlighted in Figure 10b. In Figure 10c, the typical aspect of fatigue crack is shown with the indication of striations, while Figure 10d shows the brittle aspect of the final fracture. Similar results were obtained in the welded material, and no significant differences were observed in the fractography, including in the notched samples (not shown here).

The herein presented results—along with previous results obtained by Porcaro et al.[1,11]—allows one to infer that the structural changes due to the FBW process in the analyzed steel rails, especially the partial spheroidization of cementite in the HAZ, were responsible for the significant reduction on the material fatigue resistance. Another important outcome is the high notch sensitivity presented by the steel related to the high-cycle fatigue regime. The fatigue notch sensitivity of the material—which experiences structural changes resulting from the welding process—along with the biaxial stress states with significant normal tensile residual stresses, is the main cause of HSW failure modes. Therefore, ways seeking to decrease these effects must be adopted to increase the service life and to reduce the probability of premature failures in CWRs. In the next section, an attempt to numerically describe the residual stresses arising in the FBW process is presented.
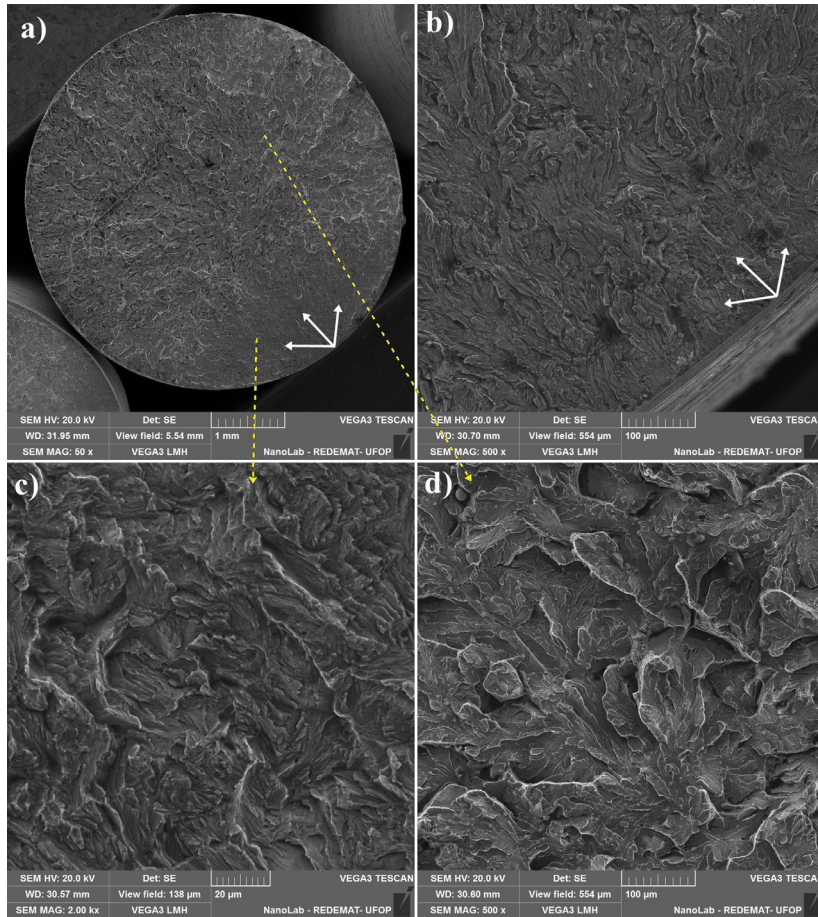

Figure 9. S-N fatigue curves for the base metal and for non-notched and notched FBW joints in intermediate pearlitic rail steel.

Figure 10. Fracture surface observation by SEM of a pearlitic rail steel with fatigue life of 50,376 cycles (stress amplitude - 314MPa). (a) Base metal. (b) Highlights of nucleation of fatigue cracks. (c) Details of the region with stable fatigue crack growth. (d) Details of the final brittle and cleavage fractures.

3.2. Numerical analysis

3.2.1. Thermal analysis

The thermal analysis results, aiming at evaluating the thermal cycles (temperature variation) during the FBW process on a TR57 rail, are shown in Figure 11a and b. Figure 11c shows the thermal cycles of three monitored points at different positions in the model, namely web surface, upper head surface, and lower foot surface. All three points were on the central line of the weld. The rail web had a maximum temperature above 1400°C. On the other hand, the rail head and the foot exhibited peak temperatures below 1350°C. These results are similar to those experimentally measured previously[8] during the FBW of a rail with a similar profile.

Other parameters monitored to adjust the heat input were the width of the heated region above 727°C and the cooling rate. In Figure 12, the width of the heated region above 727°C (A_{c1}) was greater than 40mm in the web region, which is a value slightly higher than that obtained in the metallographic analysis of this region (about 35mm[1]). Regarding the cooling rate on the surface of the model, the computationally determined values, in the range between 800°C and 500°C, were 2.90°C/s and 2.65°C/s in the rail

web and head, respectively. Weingrill et al.[8] also simulated computationally the FBW of rails and compared the numerical and experimentally measured cooling rates. Their average experimental values in the same range indicated above—between 800°C and 500°C—were around 1°C/s, whereas the simulated ones were equal to 3°C/s in the head surface. These authors attributed these differences to the material properties and/or boundary conditions used in the simulations.

From the comparison between the numerically determined temperature distribution on the welded joint at the maximum temperature, in the longitudinal section (see Figure 12b), with the corresponding macrography shown in Figure 12c, one can see a good agreement with the width of the HAZ and that obtained via macrographic measurements. It is noteworthy the larger width of the heated region in the web of the rail and close to the surfaces of the head and the foot.

According to Mansouri and Monshi[7], this nonuniform temperature distribution would be attributed to an easy transfer of electric current in the surface layers. Their idea is reasonable since they utilized a mobile machine—powered by alternating current[33]—to accomplish the flash-butt welding. However, the joints analyzed in the present study were welded by a stationary FBW machine powered by direct current.
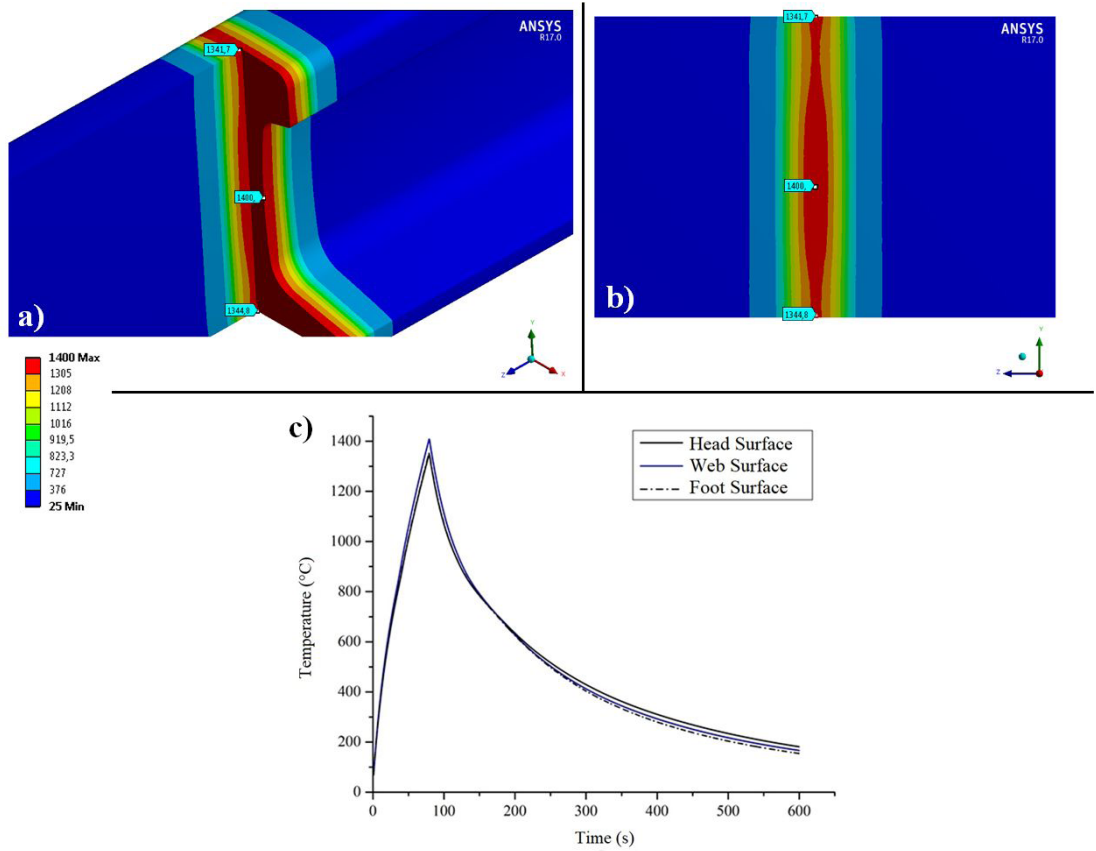
Figure 11. Temperature distribution obtained in simulations of the FBW process by the FEM. (a) and (b) Contour graph at the maximum temperature (°C). (c) Thermal cycles at the head, web and foot sections of the rail.
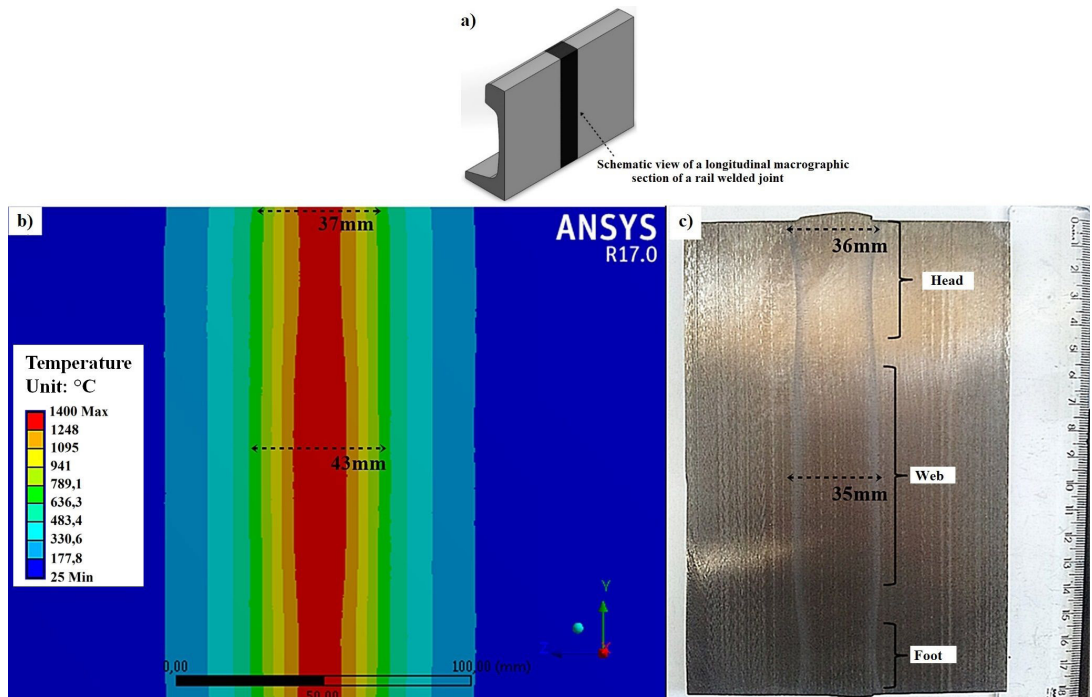

Figure 12. (a) Schematic view of the longitudinal section of the welded joint. (b) Comparison between the maximum temperature profile simulated by the FEM of the FBW and measurements of the visible HAZ in a joint. (c) Experimental measurements[1].

In this case, the electric current densities on the surface layers would not explain alone the variation in the temperature values and width of HAZ. Thus, a new hypothesis is presented here to explain the maximum temperature values and the corresponding width of HAZ close to the surface of the rail cross-section during the FBW process. Essentially, it is considered that, during the FBW, the hot burr extruded to the surface around the welding region, right after the upset force is applied, will keep the peripheral zones of the rail at higher temperatures than in its internal zones. Notice that this fact justifies the heat flow values assumed on the surface layer of the FE model (see Figure 4).

The same hypothesis explains the higher temperatures and, consequently, the larger width of the heated region (HAZ) in the rail web. Since the area/volume relationship is higher in the web than in the other zones, the heat from the hot burr is more effective in raising the rail temperature in this zone.

3.2.2. Structural analysis– residual stresses

The numerically determined normal vertical residual stresses in the rail web are presented in Figure 13a. These stress components present patterns similar to those reported in previous works—with tensile stresses in the HAZ region and compressive residual stresses in the base metal[5-7,9,23-25]. However, unlike the results reported in these previous studies, the residual stress patterns shown here are the first ones obtained considering different temperature peaks between the web, the head and the foot of the rail. The highlighted points in the web (see Figure 13a) correspond to the positions where the experimental residual stresses were measured.

It is worth noting that the Y (vertical) component of the residual stresses obtained in the simulations were similar to those reported by Skyttebol et al.[6] and Tawfik et al.[9], with values over 300MPa in the surface of the web region.

Figure 13b shows the simulated normal longitudinal component (in the Z axis direction) of the residual stresses, which were also similar to those reported in previous works, with tensile residual stress in the HAZ of the web and compressive residual stress in the surface of the rail head[6,25].

Comparisons between the numerically simulated and experimentally measured residual stresses in the web and head of the rail are given in Figures 14a, b, and c for their vertical (Y), longitudinal (Z), and transverse (X) components, respectively. A good correspondence between the experimental and numerical results can be observed, mainly in the vertical (in Y axis) direction in the web.

Differences amongst simulated and measured residual stresses in flash-butt-welded rails have also been reported by other authors[6,9,24,25]. Obvious reasons for the observed differences include simplifications in the numerical models, such as no consideration of recrystallization, lack of precise descriptions of temperature distributions (thermal cycles) inside the rail, simplifications in the material models, additional deformation effects at the end of the FBW process, and so on. Nonetheless, the computational results presented here show good agreement with the experimental ones.

The main differences between the numerical and experimental residual stresses were observed in the web of the model in the longitudinal (Z) direction. Cai et al.[23] also obtained significant differences between simulated and experimental residual longitudinal stresses in flash-butt-welded rails.
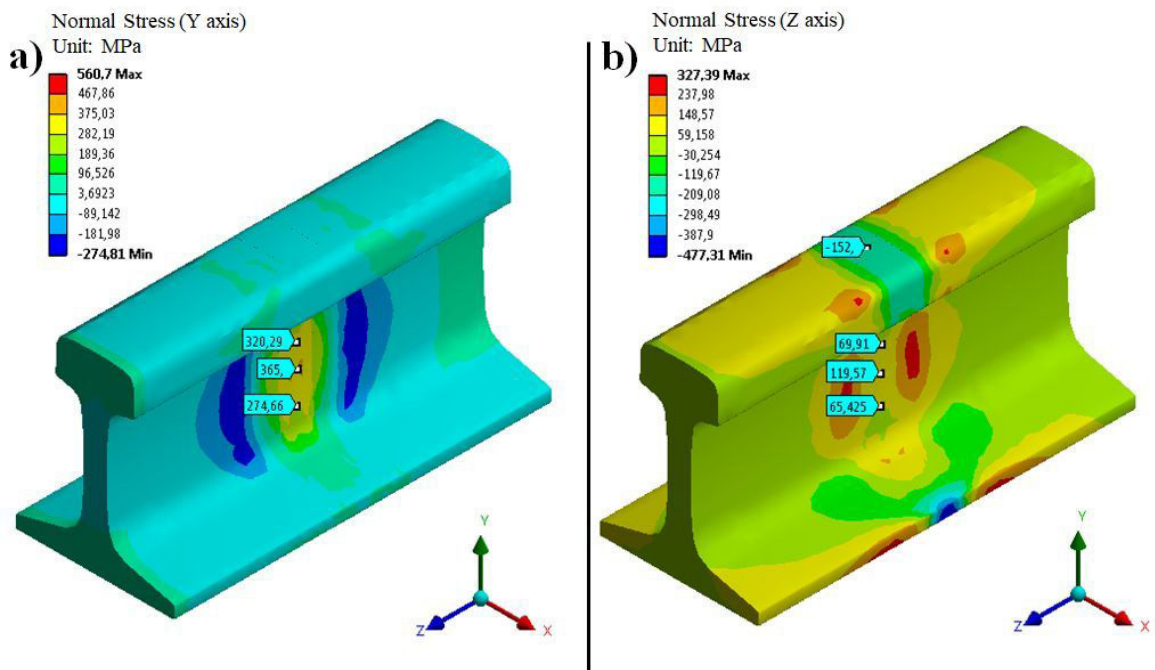

Figure 13. Normal residual stresses simulated by the FEM due to the FBW process. (a) Normal Y (vertical) component of the residual stresses. (b) Normal Z (longitudinal) component of residual stresses.

In addition to the several reasons pointed out previously for the differences between experimental and simulated residual stresses, two other factors related to the Z component of the residual stresses must be considered: (i) After the welding process, the welding burr is cut by a shearing tool that modifies the surface residual stresses in the web and, thereby, influences the experimental results. (ii) The modeling strategy adopted in previous works[6,9,23-25,34] did not consider the restraining effect of the mobile electrode during the flash-butt welding. In other words, some unknown stiffness associated with the moving electrode—the one that applies the forging load at the end of the process—should be considered. For comparison purposes, the effects of the elastic support (stiffness of moveable electrode) in the vertical and longitudinal residual stresses on the web surface are given in Figure 15a and b. As stated previously, the value of 200N/mm³ resulted in vertical stresses closer to the experimental ones—at the web surface—and was taken as standard in all models. The effects of the restriction caused by the moving electrode on the residual stresses in FBW steel rails will be further investigated in future works.
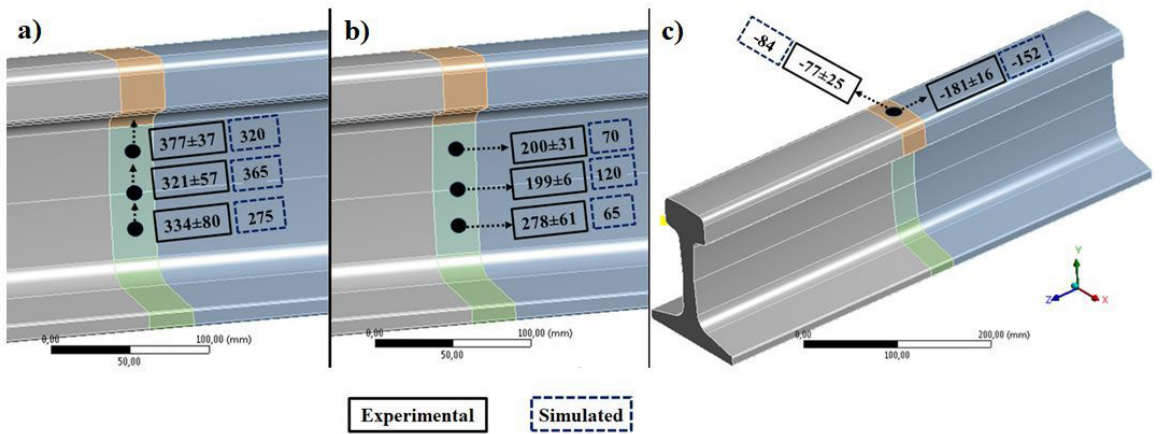

Figure 14. Comparisons between experimental and simulated normal residual stresses due to the FBW process. (a) σ_Y Y axis, (b) σ_Z Z axis, (c) σ_X X axis and σ_Z Z axis.
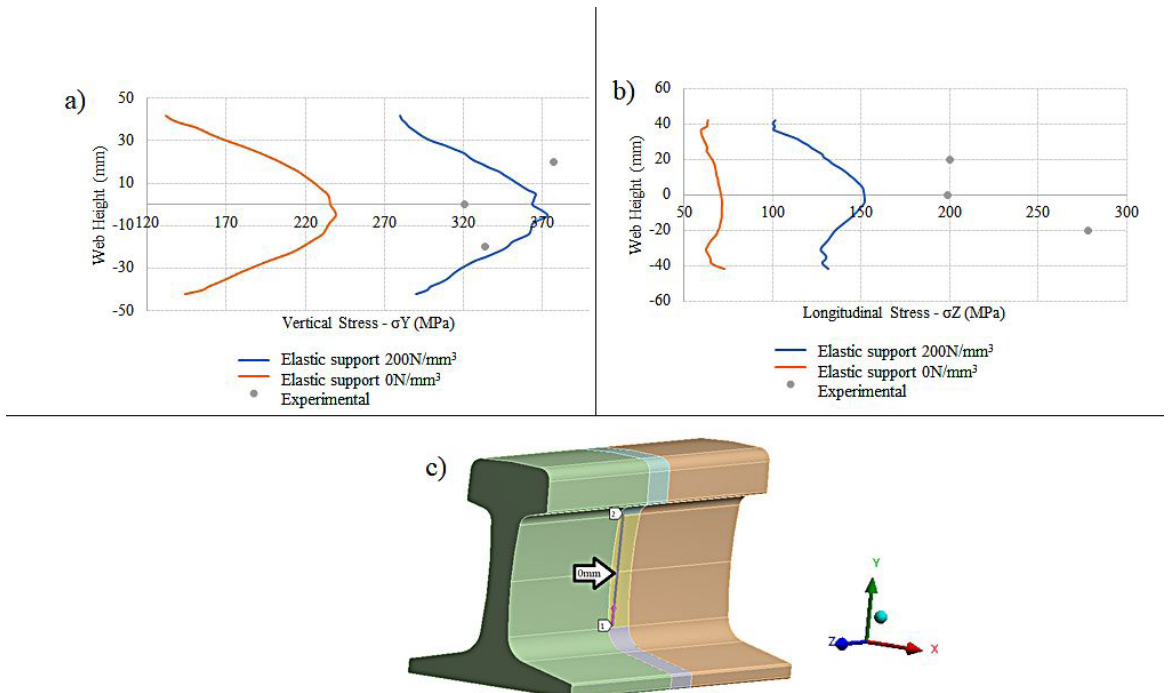

Figure 15. Effects of elastic support (stiffness of moveable electrode) in residual stresses due to the FBW process. (a) σ_Y Y axis, (b) σ_Z Z axis, (c) σ_X X axis, (c) path on the web surface in which the results were evaluated.

Stress distributions along different paths of the simulated model were compared with previous experimental and numerical works[34-36], given in Figure 16. As stated by Gedney and Rizos[34], there are few experimental data of residual stresses in flash-butt-welded rails in the technical literature. The experimental results obtained by Oliveira et al.[35] by using X-ray diffraction, came from different FBW-rail profile, rail material and welding parameters. The results from Tawfik et al.[36] have been experimentally obtained by neutron diffraction, however, in addition to being a different welding/profile/material, there was a sectioning of the weld profile prior to the analysis. Even though the models from Gedney and Rizos[34] were different from the simulation-strategy adopted in this paper, the values of residual stresses and the profiles along the paths were similar to those obtained here (Figure 16).

The vertical components of the normal residual stresses in the web are the most important physical quantities to explain the occurrence of HSW fatigue failure modes[3,9,29]. This residual stress component is generally associated with the presence of stress concentrators on the web surface that result from inadequate burr removal[1]. Furthermore, the additional stresses induced on the rails by train moving loads, especially in curved tracks, lead to nucleation and growth of early fatigue cracks as described previously[10,29]. Thus, the simulation methodology proposed here, especially the one devoted to modeling the transient heat conduction problem—which considered the heat input in the web different from that in the head and foot of the rail—can be very useful for predicting the fatigue life of FBW joints. Notice that the vertical component of tensile residual stresses on the surface of the web is crucial for determining the critical locations for nucleation of fatigue cracks.

The results obtained in a previous study[1] concerning the microstructural characterization of the material— which indicated a larger width of the HAZ in the web of welded joints—along with the thermomechanical numerical results presented here—obtained by considering, for the first time, the temperature differences between the three regions of the rail—corroborates the hypothesis according to that the presence of hot burr over the surface around the welding region, right after the upset force is applied, influences the microstructure of the material (HAZ width) and the residual stresses in welded joints. It is worth noting that the thermomechanical results presented in the present study were experimentally validated by macrographic measurements.

4. Conclusions

In this study, we accomplished the experimental characterization of flash-butt-welded joints in pearlitic rail steel focusing on the fatigue evaluation related to the HAZ and the notch sensitivity compared to the base metal. A thermomechanical model has been proposed to simulate a standard FBW welding procedure. The results, experimentally supported in the study, showed adequate reconstitution of the temperature distribution and residual stresses in flash-butt-welded joints. Besides, the following additional conclusions could be drawn:

- The obtained residual stress patterns (in the flash-butt-welded joints) showed tensile normal stresses on the surface of the rail web and compressive normal stresses on the rail head. The vertical and longitudinal stress components in the rail web were of the order of +300MPa and +200MPa, respectively, and the longitudinal and transverse stress components in the rail head were around −180MPa and −77MPa, respectively.
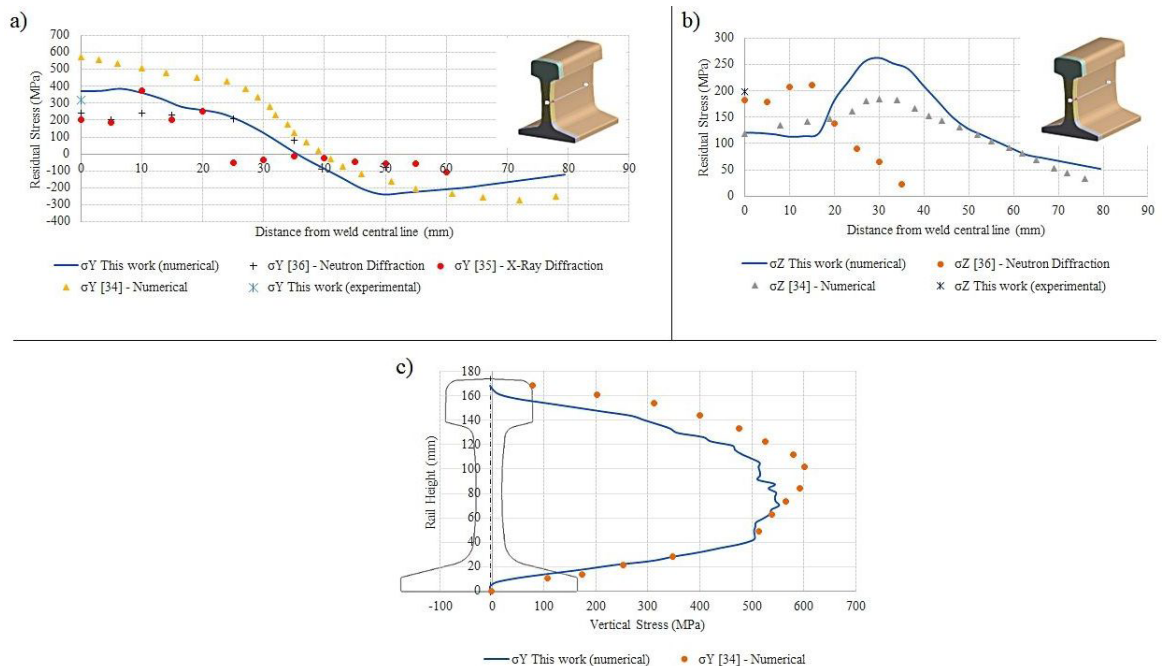

Figure 16. FBW-induced residuals stresses along paths and compared to experimental and previous works. (a) σ_Y Y axis along web surface. (b) σ_Z Z axis along web surface. (c) σ_Y Y axis, along vertical centerline path.

- Compared to the base metal, the welded joints exhibited an average decrease of 17% in yield strength and 13% in tensile strength. Besides, the welded material has proven to be highly notch sensitive in tensile tests. A decrease of 10% in the average yield strength and 8% in the tensile strength were obtained in notched welded specimens compared to non-notched welded specimens. A reduction of 60% in total elongation has been verified.
- The welding process reduced the fatigue limit of the pearlitic steel by approximately 16%. The welded joints have shown high notch sensitivity in fatigue, with a reduction by 23% of the fatigue limit related to the non-notched welded joints and by 36% related to the base metal.
- The reduction in tensile and fatigue properties of welded joints is essentially due to the partial cementite spheroidization at the end of the HAZ.
- The correct description of the volume heat source inside the weld region as well as of the prescribed heat flow on the surface of the web, the head and the foot of the rail proved to be very important for carrying out trustworthy computational simulations.
- The proposed simulation technique is quite promising for analyzing continuously welded rails (CWRs) under thermal and train moving loads and by taking into consideration fatigue effects.

5. Acknowledgements

6. References

1. Porcaro RR, Lima DAP, Faria GL, Godefroid LB, Cândido LC. Microstructure and mechanical properties of rail steel welded by flash butt welding. Soldag Insp. 2017;22(1):59-71.
2. BS: British Standards. BS EN 14587-1:2005: Railway applications. Track. Flash butt welding of rails. New R220, R260, R260Mn and R350HT grade rails in a fixed plant. Reino Unido: British Standards.
3. Farhangi H, Mousavizadeh SM. Horizontal split-web fractures of flash butt welded rails. In: 8th International Fracture Conference; 2007; Istanbul, Turkey. Proceedings. USA: Springer; 2007. p. 509-17.
4. Desimone H, Beretta S. Mechanisms of mixed mode fatigue crack propagation at rail butt-welds. Int J Fatigue. 2006;28:635-42.
5. Haibatollahi SP, Tehrani PH. Prediction of residual stress distribution in flash butt welded rails using electro-thermo-mechanical simulation. Int J Veh Struct Syst. 2013;5(2):53-7.
6. Skyttebol A, Josefson BL, Ringsberg JW. Fatigue crack growth in a welded rail under the influence of residual stresses. Eng Fract Mech. 2005;72(2):271-85.
7. Mansouri H, Monshi A. Microstructure and residual stress variations in weld zone of flash-butt welded railroads. Sci Technol Weld Join. 2004;9(3):237-46.
8. Weingrill L, Krutzler J, Enzinger N. Temperature field evolution during flash butt welding of railway rails. Mater Sci Forum. 2017;879:2088-93.
9. Tawfik D, Mutton PJ, Chiu WK. Experimental and numerical investigations: alleviating tensile residual stress in flash-butt welds by localized rapid post-weld heat treatment. J Mater Process Technol. 2008;196(1-3):279-91.
10. Godefroid LB, Faria GL, Cândido LC, Viana TG. Failure analysis of recurrent cases of fatigue fracture in flash butt welded rails. Eng Fail Anal. 2015;58(2):407-16.
11. Porcaro RP, Faria GL, Godefroid LB, Apolonio GR, Cândido LC, Pinto ES. Microstructure and mechanical properties of a flash butt welded pearlitic rail. J Mater Process Technol. 2019;270:20-7.
12. Micenko P, Muruganant A, Li H, Xiaofeng X. Double dip hardness profiles in rail weld heat-affected zone – literature and research review report. In: Micenko P, Li H, Xu X, editors. Improvements to railway welding. Brisbane, Australia: CRC for Rail Innovation; 2013. p. 1-49. Final Report.
13. Mutton P, Cookson J, Qiu C, Welsby D. Microstructural characterization of rolling contact fatigue damage in flashbutt welds. Wear. 2016;366-367:368-77.
14. Steenbergen M, Dollevoet R. On the mechanism of squat formation on train rails – part two: growth. Int J Fatigue. 2013;47:373-81.
15. Zhao X, Fan Y, Liu Y, Wang H, Dong P. Evaluation of fatigue fracture mechanism in a flash butt welding joint of a U75V type steel for railroad applications. Eng Fail Anal. 2015;55:26-38.
16. Sarikavak Y, Takeuchi T, Horiuchi T, Goda K. Experimental study of the fatigue characteristics and reliability of continuous welded rails. Fatigue Fract Eng Mater Struct. 2020;43(8):1743-54.
17. AREMA: American Railway Engineering and Maintenance-of-Way Association. Manual of railway engineering. Maryland: American Railway Engineering and Maintenance-of-Way Association; 2013.
18. ASTM: American Society for Testing and Materials. ASTM E837-13: standard test method for determining residual stresses by the role drilling strain-gage method. West Conshohocken, PA: ASTM International; 2013.
19. ASTM: American Society for Testing and Materials. ASTM E8/E8M-13: standard test methods for tension testing of metallic materials. West Conshohocken, PA: ASTM International; 2013.
20. ASTM: American Society for Testing and Materials. ASTM E466-15: standard practice for conducting force controlled constant amplitude axial fatigue tests of metallic materials. West Conshohocken, PA: ASTM International; 2015.
21. ANSYS INC. Product Launcher Release 17.0, 2016. ANSYS 17.0 Help. Canonsburg, Pensilvânia: ANSYS INC; 2016.
22. Bäker M. How to get meaningful and correct results from your finite element model. Ithaca, NY: Cornell University; 2018. [cited 2020 Apr 5]. 26 p. Available from: https://arxiv.org/abs/1811.05753
23. Cai Z, Nawafune M, Ma N, Qu Y, Cao B, Murakawa H. Residual stresses in flash butt welded rail. Trans JWRI. 2011;40:79-87.
24. Ghazanfari M, Tehrani PH. Experimental and numerical investigation of the characteristics of flash-butt joints used in continuously welded rails. Proc Inst Mech Eng F J Rail Rapid Transit. 2019;234(1):65-79.
25. Ma N, Ca Z, Huang H, Deng D, Murakawa H, Pan J. Investigation of welding residual stress in flash-butt joint of U71Mn rail steel by numerical simulation and experiment. Mater Des. 2015;88:1296-309.
26. Porcaro RR, Araújo FC, Godefroid LB, Faria GL, Silva LL. Simulation of flash-butt welding process of a railway steel. Part 1: residual stress analysis via FEM. Soldag Insp. 2019;24:1-15.
27. Tawfik D, Mutton PJ, Chiu WK. Transient thermal stress analysis on rapid post-weld heat treatments applied to flash butt welded rails. Sci Technol Weld Join. 2006;11(3):326-36.
28. Yan S, Chen H, Gou G, Li D, Liu Y, Zhu Z. Research on measurement of residual stresses in flash-butt-weld using X-ray diffraction. Adv Mat Res. 2011;291-294:934-40.

29. Godefroid LB, Faria GL, Cândido LC, Viana TG. Fatigue failure of a flash butt welded rail. Procedia Mater Sci. 2014;3:1896-901. http://dx.doi.org/10.1016/j.mspro.2014.06.306.

30. Bauri LF, Alves LHD, Pereira HB, Tschiptschin AP, Goldenstein H. The role of welding parameters on the control of the microstructure and mechanical properties of rails welded using FBW. J Mater Res Technol. 2020;9(4):8058-73.

31. Schijve J. Fatigue of structures and materials. New York: Kluwer Academic Publishers; 2001. 530 p.

32. Salehi I, Kapoor A, Mutton P. Multi-axial fatigue analysis of aluminotermic rail welds under high axle load conditions. Int J Fatigue. 2011;33:1324-36.

33. Mitsuru, F., Hiroaki, N., Kiyoshi, N. Rail flash-butt welding technology. JFE Tech Rep. 2015(20):159-63.

34. Gedney BL, Rizos DC. Combining welding-induced residual stress with thermal and mechanical stress in continuous welded rails. Results in Engineering. 2022;16:1-16.

35. Oliveira BS, Rodrigues LAS, Costa ES, Braga EM, Reis MAL. X-ray diffraction analysis of residual stresses in the premium rails welded by flash butt process. Soldag Insp. 2020;25:1-9.

36. Tawfik D, Kirstein O, Mutton PJ, Chiu WK. Verification of residual stresses in flash-butt-weld rails using neutron diffraction. Phys B Condens Matter. 2006;385-386(Pt 2):894-6. https://doi.org/10.1016/j.physb.2006.05.242.